CHEMISTRY OF
MATERIALS
Article

Chem. Mater. **2010,** *22,* 3843–3853 3843
DOI:10.1021/cm903260f

Highly Visible Light Active $TiO_{2-x}N_x$ Heterojunction Photocatalysts[†]

Vinodkumar Etacheri,[‡,§] Michael K. Seery,[§] Steven J. Hinder,[‖] and Suresh C. Pillai*[,‡]

[‡]*Centre for Research in Engineering Surface Technology (CREST), FOCAS Institute, and*
[§]*School of Chemical and Pharmaceutical Sciences, Dublin Institute of Technology, Kevin Street, Dublin 8, Ireland, and* [‖]*The Surface Analysis Laboratory, Faculty of Engineering and Physical Sciences, University of Surrey, Guildford, Surrey, GU2 7XH, United Kingdom*

Received October 23, 2009. Revised Manuscript Received May 10, 2010

Nitrogen doped anatase-rutile heterojunctions are successfully synthesized through an ethylenediaminetetraacetic acid (EDTA) modified sol−gel process. An FT-IR study of EDTA modified TiO_2 gel confirms the existence of an ionic intermediate (as indicated by a $\Delta\nu$ value of 233 cm^{-1}). Differential scanning calorimetry (DSC), X-ray diffraction (XRD), and Raman spectroscopy are employed to study the phase evolution, phase purity, and crystallite size of samples. Formations of O−Ti−N and N−Ti−N bonds in calcined samples are confirmed using XPS and FT-IR spectroscopy. All EDTA modified samples show significantly higher visible light photocatalytic activity than the unmodified sample. The most active nitrogen doped heterojunction obtained at 400 °C exhibits 9-fold visible light activity in comparison to the standard photocatalyst Degussa P-25. It is proposed that the photo excited electrons (from the visible midgap level) are effectively transferred from the conduction band of anatase to that of rutile causing effective electron−hole separation, which is responsible for the higher visible light activity and lower photoluminescence (PL) intensity.

1. Introduction

Unique properties of nanosized catalysts such as quantum confinement and high surface to volume ratio make them highly efficient. Among various catalysts, titania nanomaterials find wide applications in the field of solar cells,[1] organic synthesis,[2] water and air purification,[3] cancer therapy,[4] cathodic corrosion protection, and self-cleaning antibacterial materials.[5,6] High redox potential, chemical stability, inexpensiveness, and non toxicity of titania made it superior to other semiconductor photocatalysts in its class. Among the three polymorphs, it is generally agreed that the anatase phase has the highest photoactivity followed by rutile and brookite. The efficiency of titania photocatalysts strongly depends on several factors, including phase purity, surface area, crystallite size, amount and nature of dopants, method of preparation, and anatase-rutile ratio.[7−9]

The wide band gap (3.2 eV) of the anatase titania confines its application to UV light ($\lambda \leq 387.5$ nm) activation. Even though the high temperature stable rutile phase can absorb visible light (up to ~412 nm), its activity is limited as a result of low surface area, low redox potential, and faster electron hole recombination rate.[10] The development of a highly visible light active catalyst is necessary to effectively exploit sunlight or light from artificial sources. Various methods such as metal or non-metal doping, using reduced forms of TiO_X ($X < 2$) photocatalyst, dye sensitization, and optimization of phase composition has been investigated by previous researchers.[11−13]

Titania doped with main group elements has attracted great interest after the report of nitrogen and other anion (S, C, and F) doped visible-light active (VLA) titania catalyst by Asahi and co-workers.[14] These second-generation TiO_2 materials were photoactive over the UV and visible-light region. Controversy still remains about the nature of the dopant species and electronic structure of nitrogen doped titania, which is highly dependent on the method of preparation. Some researchers proposed the existence of surface adsorbed NO_X and NH_X, while others proposed the presence of lattice nitrogen. Recently, Valentine et al. demonstrated the electronic structure of nitrogen doped

---

[†] This paper is dedicated to Professor John M. Kelly, C. Chem. FRSC on the occasion of completing his 37 years of teaching and research (celebration of chemistry) at the Trinity College Dublin, Ireland.

*To whom correspondence should be addressed. E-mail: suresh.pillai@dit.ie.

(1) O'Regan, B.; Grätzel, M. *Nature* **1991**, *353*, 737.
(2) Kraeutler, B.; Bard, A. J. *J. Am. Chem. Soc.* **1978**, *100*, 2239.
(3) Ollis, D. F.; Al-Ekabi, H. *Photocatalytic Purification and Treatment of Water and Air*; Elsevier: Amsterdam, The Netherlands, 1993.
(4) Cai, R.; Kubota, Y.; Shuin, T.; Sakai, H.; Hashimoto, K.; Fujishima, A. *Cancer Res.* **1992**, *52*, 2346.
(5) Yuan, J.; Tsujikawa, S. *J. Electrochem. Soc.* **1995**, *142*, 3444.
(6) Honda, H.; Ishizaki, A.; Soma, R.; Hashimoto, K.; Fujishima, A. *J. Illum. Eng. Soc.* **1998**, 42.
(7) Kavan, L.; Grätzel, M.; Gilbert, S. E.; Klemenz, C.; Scheel, H. J. *J. Am. Chem. Soc.* **1996**, *118*, 6716–6723.
(8) Toyoda, M.; Nanbu, Y.; Nakazawa, Y.; Hirano, M.; Inagaki, M. *Appl. Catal., B* **2004**, *49*, 227.
(9) Beyers, E.; Cool, P.; Vansant, E. F. *J. Phys. Chem. B* **2005**, *109*, 10081.
(10) Miyagi, T.; Kamei, M.; Mitsuhashi, T.; Ishigaki, T.; Yamazaki, A. *Chem. Phys. Lett.* **2004**, *390*, 399–402.
(11) Kang, M. G.; Park, N. G.; Park, Y. J.; Ryu, K. S.; Chang, S. H. *Sol. Energy Mater. Sol. Cells* **2003**, *75*, 475.
(12) Siemon, U.; Bahnemann, D.; Testa, J. J.; Rodŕguez, D.; Litter, M. I.; Bruno, N. *J. Photochem. Photobiol., A* **2002**, *148*, 247.
(13) Nakamura, I.; Negishi, N.; Kutsuna, S.; Ihara, T.; Sugihara, S.; Takeuchi, K. *J. Mol. Catal. A: qChem.* **2000**, *161*, 205.
(14) Asahi, R.; Morikawa, T.; Ohwaki, T.; Aoki, K.; Taga, Y. *Science* **2001**, *293*, 269–275.

titania synthesized through various routes.[15] Density functional theory (DFT) calculations show that substitutional nitrogen atoms create an energy level just above the valence band, where as interstitial nitrogen energy levels lie higher in the gap. Calculations also showed that nitrogen doping leads to an ample lowering of oxygen vacancy formation energy. Photoelectrochemical studies of nitrogen doped titania revealed the formation of additional energy states positioned energetically 1.3 eV broad range just below the conduction band edge. These energy levels cause higher loss of visible light excited charge carriers as a result of recombination.[16] Increasing the doping density also enhances the electron−hole recombination as a result of the reduced band gap. These main drawbacks of nitrogen doped titania limit its visible light activity and applications. For efficient visible light photocatalysis, coupling of nitrogen doped titania with the electron hole separating agents are necessary.

One way to attain high activity is proper designing of heterojunctions with smaller band gap semiconductors, such as rutile. A mixture of anatase and rutile can often outperform the photoactivity of pure anatase or rutile. Recent studies explained the visible light induced production of charges in smaller band gap rutile phase and its transfer to the trapping states of anatase phase.[17] Since the conduction band level of rutile is below that of anatase, photo generated electrons from the conduction band of anatase can be effectively transferred to that of rutile leading to slow electron hole recombination.[7,18] These two key factors are reported to be responsible for the superior photocatalytic activity of Degussa P25, which has an anatase-rutile ratio of 70/30.[19] Most of the synthesis methods of titania gives anatase rutile mixtures only above 600 °C resulting in a deviation from nanoregime and a subsequent decrease in photocatalytic activity. Nitrogen doping also results in the formation of high temperature stable anatase phase titania.[20−22] Under these circumstances, it is necessary to develop a low temperature method for the synthesis of nitrogen doped anatase-rutile nano heterojunctions. This has been achieved through an ethylenediaminetetraacetic acid (EDTA) modified sol−gel process, which proceeds through an ionic intermediate [Ti (H_2O) (edta)]. This method proceeds through a solution phase without the formation of polymeric chains, which can ensure better homogeneity and effective doping than conventional sol−gel processes. Both low temperature crystallizations of anatase-rutile heterojunctions and nitrogen doping were achieved using EDTA. Nishide et al. studied the crystal structure and optical properties of TiO_2 materials prepared from Ti-EDTA complexes.[23] High photocatalytic activities of anatase-brookite and anatase-carbon nanotubes heterojunctions have also been reported.[24,25] However, to the best of our knowledge, there is no systematic study available on a highly visible light active $TiO_{2-x}N_x$ anatase-rutile heterojunction photocatalysts. The current study focuses on the low temperature crystallization, mechanism of formation, and the photocatalytic activity of $TiO_{2-x}N_x$ heterojunctions.

2. Experimental Methods

2.1. Synthesis of N-Doped Titania Heterojunctions. All reagents were used without further purification. Titanium isopropoxide (Aldrich 97%) and EDTA (Aldrich 99.99%) was used as the titania precursor and modifier respectively. In a typical synthesis for 1:1 EDTA modified sample, titanium isopropoxide (9 mL) was dissolved in isopropanol (23 mL). This solution was mixed with glacial acetic acid (1.7 mL) and EDTA (8.8 g). The precipitate obtained was then mixed with deionized water (55 mL) and stirred for 2 h to form a sol. The sol obtained was then heated in an oven at 80 °C to form a solution, which on further heating converts to a gel. Xerogel thus obtained after 24 h was calcined at 400, 500, 600, 700, 800, and 900 °C for 2 h at a heating rate of 10 °C/min. Various molar ratios of TTIP/IPA/ACOH/H_2O/EDTA were used for the synthesis of different samples (Supporting Information 15). All nitrogen doped heterojunctions were prepared by successively replacing 0.5 molar ratios of acetic acid by EDTA (identified as 0.5 ED-TiO_2, 1.0 ED-TiO_2, 1.5 ED-TiO_2, and 2.0 ED-TiO_2 respectively after calcination). Ratios between other reagents were maintained as constant in all synthesis. The control sample without EDTA was also prepared using the same synthesis method. Molar ratio between titanium isopropoxide, acetic acid, isopropanol, and water was 1:2:10:100 for the synthesis of the control sample. Degussa P-25 was used as the standard TiO_2 sample for comparison.

2.2. Characterization Techniques. The FTIR spectra of xerogel dried at 100 °C and calcined at different temperatures were recorded using a Perkin-Elmer GX-FTIR spectrometer in the range 4000−400 cm^{-1}. Transparent pellets were prepared using a 4 mm dye after mixing samples with KBr. Rheometric Scientific DSC QC and Shimadzu DTG-60 instruments were used for differential scanning calorimetry (DSC) and differential thermal analysis (DTA) respectively. In both cases, about 5 mg of dried gel was heated from room temperature (25 °C) to 600 °C at a constant heating rate of 10 °C/min. The crystal phases of calcined samples were analyzed by X-ray diffraction using a Siemens D500 X-ray diffractometer ($2\theta = 10-70°$) working with Cu−Kα radiation ($\lambda = 0.15418$ nm). The Spurr equation (eq 1) was employed for the precise calculation of the amount of rutile in the sample.

$$F_R = \frac{1}{1 + 0.8[I_A(101)/I_R(110)]} \tag{1}$$

---

(15) Valentin, C. D.; Pacchioni, G.; Selloni, A.; Livraghi, S.; Giamello, E. *J. Phys. Chem. B* **2005**, *109*, 11414–11419.

(16) Torres, G. R.; Lindgren, T.; Lu, J.; Granqvist, C.-G.; Lindquist, S.-E. *J. Phys. Chem. B* **2004**, *108*, 5995–6003.

(17) Junin, C.; Thanachayanont, C.; Euvananont, C.; Inpor, K.; Limthongkul, P. *Eur. J. Inorg. Chem.* **2008**, 974–979.

(18) Kawahara, T.; Konishi, Y.; Tada, H.; Tohge, N.; Nishii, J.; Ito, S. *Angew. Chem., Int. Ed.* **2002**, *41*(15), 2811–2813.

(19) Balasubramanian, G.; Dionysiou, D. D.; Suidan, M. T.; Baudin, I.; Laine, J. M. *Appl. Catal., B* **2004**, *47*, 73–84.

(20) Pillai, S. C.; Periyat, P.; George, R.; McCormack, D. E.; Seery, M. K.; Hayden, H.; Colreavy, J.; Corr, D.; Hinder, S. J. *J. Phys. Chem. C* **2007**, *111*, 1605–1611.

(21) Sato, S.; Nakamura, R.; Abe, S. *Appl. Catal., A* **2005**, *284*, 131.

(22) Mwabora, J. M.; Lindgren, T.; Avendano, E.; Jaramillo, T. F.; Lu, J.; Lindquist, S. E.; Granqvist, C. G. *J. Phys. Chem. B* **2004**, *108*, 20193.

(23) Nishide, T.; Sato, M.; Hara, H. *J. Mater. Sci.* **2000**, *35*, 465–469.

(24) Tian, G.; Fu, H.; Jing, L.; Xin, B.; Pan, K. *J. Phys. Chem. C* **2008**, *112*, 3083–3089.

(25) Wang, H.; Quan, X.; Yu, H.; Chen, S. *Carbon* **2008**, *46*, 1126–1132.

Where F_R is the mass fraction of rutile, $I_A(1\,0\,1)$ and $I_R(1\,1\,0)$ are the integrated main peak intensities of anatase and rutile, respectively. Crystallite sizes of anatase and rutile in calcined samples were calculated using the Scherrer equation (eq 2).

$$\Phi = \frac{k\lambda}{\beta \cos \theta} \qquad (2)$$

Where Φ is the crystallite size, k is the shape factor, λ is the X-ray radiation wavelength, and β the full line width at half-maximum height of the main intensity peak after subtraction of the equipment line broadening. Raman spectra of all samples were recorded at room temperature with a Dilor ISA Labram 1 B micro-Raman system equipped with a 514 nm Ar^+ ion laser (Laser Physics Reliant 150 Select Multi-Line). Measurements were carried out on powder samples at a laser power of 3 mW to avoid excessive heating.

X-ray photoelectron spectroscopy (XPS) analyses were performed on a Thermo VG Scientific Sigma Probe spectrometer using monochromatic Al−Kα radiation (photon energy 1486.6 eV). For Ti 2p high-resolution spectra pass energy of 20 eV and a 0.1 eV step size were used. A pass energy of 50 eV and a step size of 0.2 eV were used for N 1s high-resolution spectra. Charge compensation was achieved by using a low-energy electron flood gun. Quantitative surface chemical analyses were calculated from the high-resolution core level spectra, following the removal of a nonlinear Shirley background. Absorbance spectra of the samples were recorded in the diffuse reflectance mode (with an integrated sphere attachment) using a Perkin-Elmer Lambda 900 UV/vis/NIR spectrometer, using $BaSO_4$ as the reference sample (in the range of 300−600 nm). Sample pellets were prepared using a 4 mm die after thoroughly mixing the powder samples with KBr. The band gaps were calculated by extrapolating the lower wavelength cutoff region. Samples for photoluminescence studies were prepared by dispersing as prepared powders (0.01 g in 100 mL) in deionized water. All samples were sonicated for 30 min before analysis. Room temperature emission spectra of samples were obtained from Perkin-Elmer Luminescence Spectrometer (LS-55) at an excitation wavelength of 260 nm in the range 300 to 800 nm.

Nitrogen adsorption and desorption isotherms were collected at liquid nitrogen temperature using a Quantachrome 2000e surface area analyzer. All samples were degassed at 300 °C for 2 h under vacuum prior to the analysis. The specific surface area was calculated using the linear portion of the Brunauer−Emmett−Teller (BET) model ($P/P_0 = 0.05{-}0.2$). Desorption branch of the Barret−Joyner−Halenda (BJH) model was employed for the precise determination of pore diameter and volumes. For transmission electron microscopy (TEM) analysis, powder samples were suspended in water and sonicated for 30 min before being dispersed onto Formvar-coated copper grids. The particle-loaded grids were studied under JEOL JEM-2100 transmission electron microscope operating at an accelerating voltage of 200 kV.

2.3. Photocatalysis Study. Decomposition of methylene blue was performed to evaluate the photocatalytic activities of samples. The catalyst (0.06 g) was dispersed in an aqueous solution of methylene blue (50 mL 1×10^{-5} M) placed in a glass vessel (100 mL). The vessel was placed in the dark for 30 min and irradiated with visible light (0.68 W/m^2) using Q-Sun solar simulator and a primary blue filter (450 nm) (Supporting Information 13). The temperature of the suspension was maintained at 25 °C with the help of an air cooler (thermostat attached) connected to the solar simulator. Degradation of methylene blue was monitored by taking aliquots at equal time intervals of 1 h. These aliquots were centrifuged, and absorption spectra of the samples were recorded using Perkin-Elmer Lambda 900 UV/vis/NIR spectrometer. Similar experiments were carried out for samples calcined at different temperatures. The rate of degradation was assumed to obey pseudo-first order kinetics, given that natural logarithmic plots were linear. The rate constant for degradation, k, was calculated from the first order plot (eq 3).

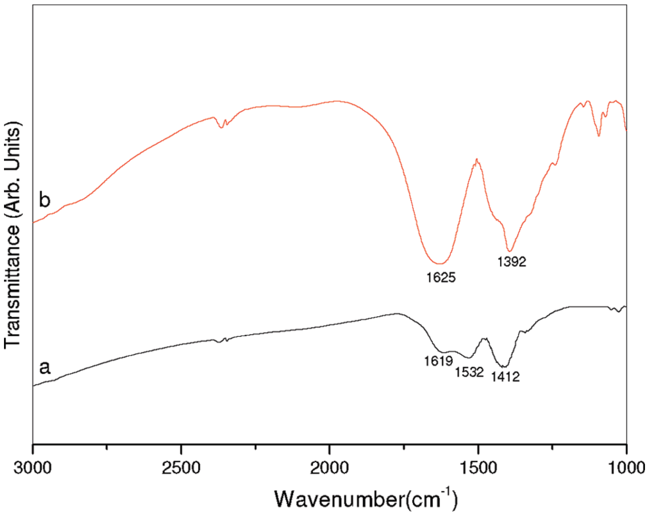

Figure 1. FT-IR Spectrum of 80 °C dried titania precursor (a) acetic acid modified and (b) EDTA modified.

$$\ln\left(\frac{A_0}{A}\right) = kt \qquad (3)$$

Where A_0 is the initial absorbance, A is absorbance after a time (t), and k is the first order rate constant. All photocatalytic experiments were triplicated, and the rate constants were within 5% error limit.

3. Results and Discussion

3.1. Characterization of Modified Precursor. *3.1.1. FT-IR Spectral Studies.* The nature of reaction intermediates formed from acetic acid and EDTA modified titania precursor was investigated using FT-IR spectroscopy. Formation of an ionic Ti-EDTA complex responsible for the low temperature crystallization of heterojunctions was observed from this study. The difference in frequency $\Delta\nu$ between antisymmetric and symmetric vibrations of C=O bonds are usually related to the type of coordination (Figure 1) in metal carboxylates.[26] Acetic acid modified gel exhibits characteristic antisymmetric and symmetric C=O stretching vibrations at 1532 and 1412 cm^{-1}, respectively.[27,28] The $\Delta\nu$ value of 120 cm^{-1} observed is characteristic of a bridged acetic acid titanium isopropoxide complex as reported by Sanchez et al.[28] Antisymmetric and symmetric C=O stretching vibrations of EDTA modified

---

(26) Mehrotra, R. C.; Bohra, R. *Metal Carboxylates*; Academic Press: London, 1983; p 48.

(27) Perrin, F. X.; Nguyen, V.; Vernet, J. L. *J. Sol-Gel Sci. Technol.* **2003**, *28*, 205–215.

(28) Doeuff, S.; Henry, M.; Sanchez, C.; Livage, J. *J. Non-Cryst. Solids* **1987**, *89*, 206–216.

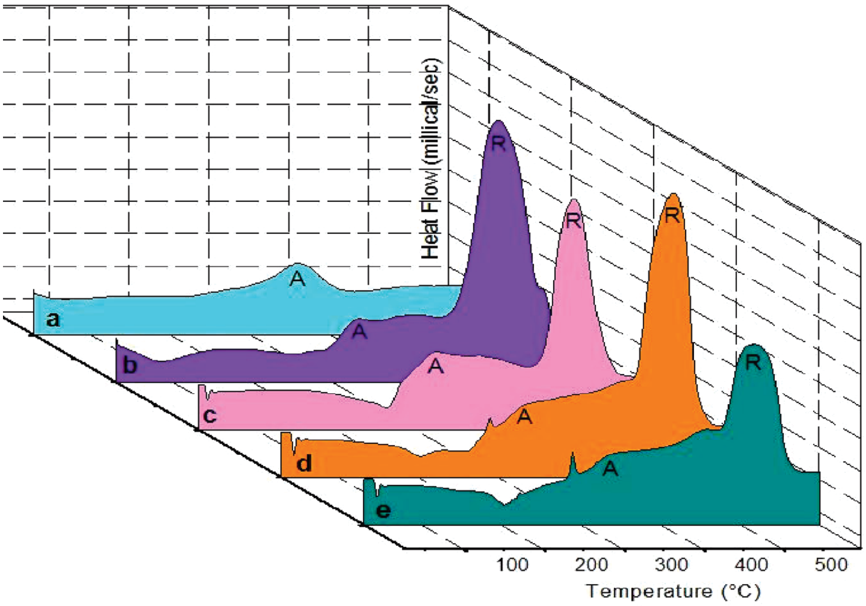

Figure 2. Differential scanning calorimetric pattern of titania gel. (a) Control sample, (b) 0.5 ED-TiO_2, (c) 1.0 ED-TiO_2, (d) 1.5 ED-TiO_2, (e) 2.0 ED-TiO_2.

gel were found at 1625 and 1392 cm^{-1}, respectively. The $\Delta\nu$ value of 233 cm^{-1} observed for the EDTA modified gel confirmed the monodentate and ionic behavior of COO group in the complex.[29] The spectrum of this complex was consistent with that of [Ti (H_2O) (edta)] as observed by Sato et al.[30]

All EDTA modified samples showed identical FT-IR spectra. The formation of the acetic acid bridged complex was not observed in compositions containing both acetic acid and EDTA. These results indicate a preferential formation of the [Ti (H_2O) (edta)] complex from a mixture of acetic acid, EDTA, and titanium tetraisopropoxide, which can be correlated to the stronger ligand character of EDTA. Variations of ionic character among the different EDTA modified compositions were also investigated. An increase of ionic character was observed as a decrease in antisymmetric stretching frequency values of C=O group (Supporting Information 1). A minimum antisymmetric value of 1600 cm^{-1} observed for 1:1 EDTA complex indicates it is of the highest ionic character, leading to a lowest thermal stability. This was later confirmed by the completion of phase transformation to rutile at 700 °C (From XRD). Bridged acetate groups in the acetic acid complex effectively alter the condensation pathway and promote the formation of linear polymers. This leads to the formation of anatase titania at higher temperatures, whereas EDTA complex exists as monomers resulting in the low temperature crystallization of anatase and rutile. These results thus confirmed the formation of a high temperature stable covalent acetic acid complex and a thermally less stable ionic EDTA complex of Ti^{4+} (Supporting Information 2).

3.1.2. Thermal Stability Analysis of Modified Precursor. Both the amorphous to anatase transition and the anatase-rutile transformation (ART) from acetic acid and EDTA derived complexes of titania were analyzed using differential scanning calorimetry (DSC) and thermogravimetric analysis (TGA) techniques. For both samples, evaporation of water and acetic acid molecules from the gel was observed as an endothermic DSC peak at 50 °C (Figure 2). The acetic acid complex showed only one exothermic peak at 360 °C representing the crystallization of anatase phase. Anatase to rutile transformation was not observed for this complex up to 600 °C. Removal of coordinated water molecules from the EDTA complexes were observed as an endothermic peak at 265 °C. Since there are no such coordinated water molecules in acetic acid complex, a corresponding peak was not observed in these samples. Among the different EDTA complexes, the most ionic (1:1 EDTA) material shows the lowest anatase and rutile crystallization temperatures of 320 and 498 °C respectively. Slight increases in both temperatures were observed for complexes containing excess EDTA (1:1.5 and 1:2). This may be due to the hindering effect of excess EDTA toward anatase phase evolution and its transformation to rutile. An additional exotherm responsible for the decomposition of unreacted EDTA was also observed at 290 °C in complexes containing excess EDTA (1:1.5 and 1:2).[31] The formation of anatase-rutile heterojunctions were observed only from EDTA modified titania precursor. In contrast, acetic acid modified precursor shows higher thermal stability. It is thus clear that in the case of EDTA modified samples, amorphous to crystalline as well as anatase to rutile transformations happened at lower temperatures.

The total weight loss calculated for the acetic acid modified complex from the TGA curve was 17%. An increased weight loss of 58% and 85% was observed for 1:0.5 and 1:2.0 EDTA modified compositions respectively

---

(29) Sawyer, D. T.; MCKinnie, M. *Inorg. Chem.* **1960**, *82*, 4191–4196.

(30) Sato, M.; Hara, H.; Nishide, T.; Sawada, Y. *J. Mater. Chem.* **1996**, *6*(11), 1767–1770.

(31) Guinesi, L. S.; Ribeiro, C. A.; Crespi, M. S.; Santos, A. F.; Capela, M. V. *J. Therm. Anal. Calorim.* **2006**, *85*, 301–307.

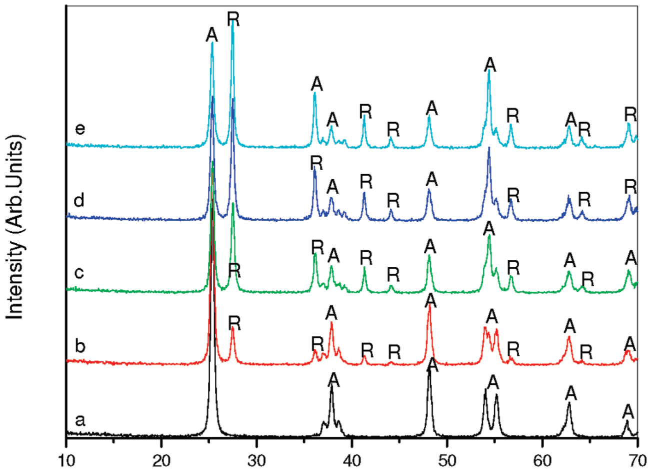

Figure 3. XRD of samples calcined at 600 °C. (a) Control TiO_2, (b) 0.5 ED-TiO_2, (c) 1.0 ED-TiO_2, (d) 1.5 ED-TiO_2, (e) 2.0 ED-TiO_2 (A = anatase; R = rutile).

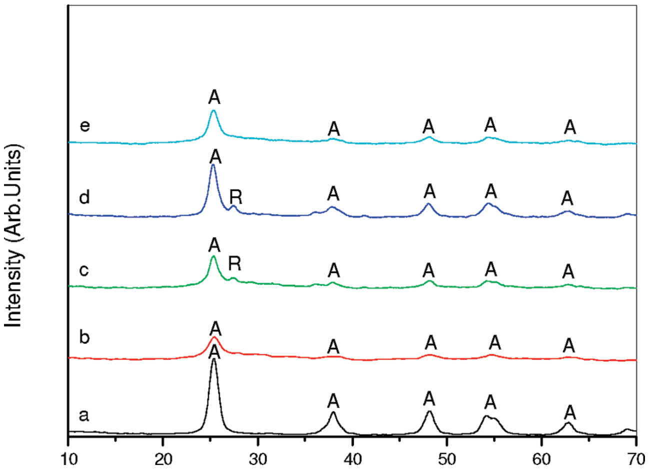

Figure 4. XRD of samples calcined at 400 °C. (a) Control TiO_2, (b) 0.5 ED-TiO_2, (c) 1.0 ED-TiO_2 ,(d) 1.5 ED-TiO_2, (e) 2.0 ED-TiO_2 (A = anatase; R = rutile).

(Supporting Information 3). The weight losses for the acetic acid complex happen in the range 30−250 °C and 300−500 °C because of the evaporation of solvents and the decomposition of the complex into crystalline anatase titania. On the other hand, the EDTA complex decomposes in three steps (30−150, 250−450, 530−600 °C), a process corresponding to evaporation of solvents, decomposition of EDTA-titania complex in to anatase titania, and anatase-rutile transformation, respectively. On increasing the amount of EDTA, a significant increased weight loss in the anatase formation step was observed, which can be due to the decomposition of excess EDTA present in these samples. The lowering of both the anatase and rutile formation temperature was also observed (from the TGA curve) on increasing the amount of EDTA.

3.2. Formation of N-Doped Heterojunctions. *3.2.1. X-ray Diffraction Studies.* X-ray diffraction patterns recorded from samples calcined at different temperatures confirmed the high temperature stability of acetic acid modified samples and low temperature crystallization of N-doped anatase-rutile heterojunctions from EDTA modified samples. The control sample showed only the peaks characteristic of anatase phase up to 600 °C (Figure 3), whereas all EDTA modified samples exist as anatase-rutile mixtures at a temperature as low as 500 °C. The crystallization of anatase-rutile heterojunctions were observed even at 400 °C for 1:1 and 1:1.5 EDTA modified samples (Figure 4). Complete rutile formation for the 1:1 EDTA modified sample (which was found to be the most ionic from FT-IR studies) was observed at 700 °C (Supporting Information 4). Compared to other EDTA modified samples, 1:2.0 modified EDTA sample shows slow anatase rutile transformation kinetics and contains 4% anatase even at 800 °C. All samples calcined at 900 °C exist as 100% rutile (Supporting Information 5). Bridged acetate groups in AcOH-Ti complex effectively alter the condensation pathway and promote the formation of linear polymers. This leads to the formation of anatase titania at higher temperatures, whereas EDTA-Ti complex exists as monomers and results in the low temperature crystallization of both anatase and rutile phases having large crystallite sizes. Slight changes (2θ = 0.2°) in the anatase 110 peak positions for EDTA modified titania samples were observed even at 400 °C compared to the control sample (Supporting Information 6), which results from changes in the lattice parameters as a result of nitrogen doping.[32] Thus XRD results revealed the low temperature crystallization of anatase rutile heterojunctions from EDTA modified titania samples and successful lattice incorporation of nitrogen.

3.2.2. Raman Studies. Raman spectroscopy, a more surface sensitive technique was employed as an additional tool to confirm phase composition and surface homogeneity.[33] The Raman active modes for anatase (A_{1g}+$2B_{1g}$+$3E_g$ at 147, 197, 396, 516, and 638 cm^{-1}) and rutile (A_{1g}+B_{1g}+B_{2g}+E_g at 144, 238, 447, and 611 cm^{-1}) were used as fingerprints.[34−36] The samples 1:1 EDTA and 1:1.5 EDTA calcined at 400 °C has peaks characteristic of anatase rutile mixtures, while other samples show peaks of pure anatase phase (Supporting Information 7). Only the acetic acid modified sample gives peaks of anatase at 600 °C; all EDTA modified samples were anatase-rutile mixtures (Figure 5). All samples calcined at 900 °C shows peaks at 144, 611, 447, and 238 cm^{-1}, which confirmed the existence of 100% rutile phase (Supporting Information 8). Thus the results observed from X-ray diffraction studies were further confirmed by Raman spectroscopy.

3.2.3. FT-IR Spectral Studies. Spectra of heterojunctions obtained were highly dependent on the processing temperature and nature of dopant species (Figure 6). Considerable shifting of Ti−O−Ti stretching frequencies to higher energy was observed for N-doped samples in comparison to the undoped one. At 400 °C, Ti−O−Ti stretching peak of N-doped sample was observed at a

---

(32) Zhang, Q.; Gao, L. *J. Eur. Ceram. Soc.* **2006**, *26*, 1535–1545.
(33) Gao, K. *Phys. B* **2007**, *398*, 33–37.
(34) Ohsaka, T.; Izumi, F.; Fujiki, Y. *J. Raman Spectrosc.* **1978**, *7*, 321.
(35) Berger, H.; Tang, H.; Lévy, F. *J. Cryst. Growth* **1993**, *130*, 108.
(36) Tang, H.; Prasad, K.; Sanjines, R.; Schmid, P. E.; Levy, F. *J. Appl. Phys.* **1994**, *75*, 2042.

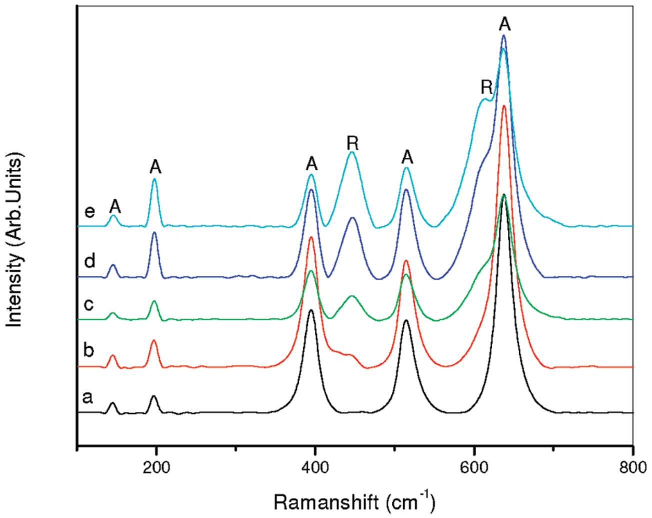

Figure 5. Raman spectra of samples calcined at 600 °C. (a) Control TiO_2, (b) 0.5 ED-TiO_2, (c) 1.0 ED-TiO_2, (d) 1.5 ED-TiO_2, (e) 2.0 ED-TiO_2.

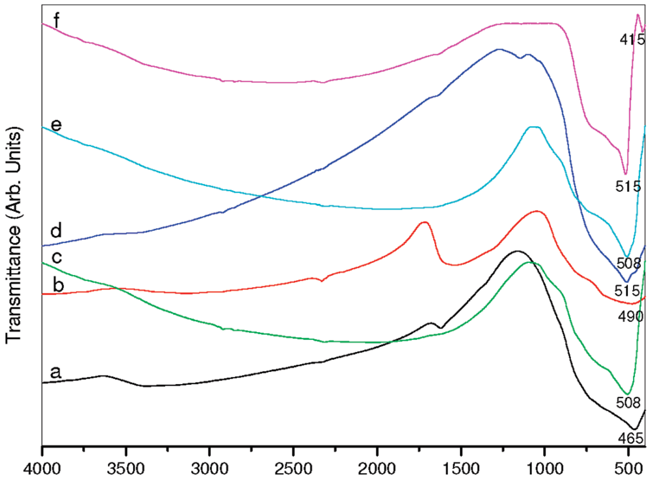

Figure 6. FT-IR Spectrum of calcined titania. (a) Control TiO_2 400, (b) 0.5 ED-TiO_2 400, (c) Control TiO_2 600, (d) 0.5 ED-TiO_2 600, (e) Control TiO_2 700, (f) 0.5 ED-TiO_2 700.

higher energy of 508 cm^{-1} compared to 465 cm^{-1} for undoped one. Similar shift in Ti−O−Ti stretching energies were also observed for samples calcined at higher temperatures. These types of shifts to higher energies were previously reported and assigned to the formation of O−Ti−N and N−Ti−N bonds in N-doped titania.[37] Since we observed the formation of N−Ti−N bonds as an additional peak at 415 cm^{-1} in samples calcined at 700 °C,[37] shifting observed for Ti−O−Ti stretching energies below this temperature can be assigned to the formation of O−Ti−N bonds through partial replacement of oxygen. No evidence for interstitial nitrogen doping and other nitrogen impurities were observed from the spectra. The lattice incorporation of nitrogen in two different forms was thus observed from FT-IR results. Formations of O−Ti−N and N−Ti−N bonds were also confirmed through XPS studies and will be discussed in the following section.

3.2.4. XPS Studies. XPS results revealed two types of lattice doping (O−Ti−N and N−Ti−N) and a decrease of nitrogen content with an increase of EDTA concentration (Supporting Information 9). An increase of EDTA concentration accelerates crystallite growth (from XRD results), which can decrease the amount N-doping as a result of surface and lattice strain relaxation. Decrease of nitrogen content was also observed with an increase of calcination temperature. This can be due to the crystallite growth and escape of the dopant species formed through the decomposition of Ti-EDTA complex at higher temperatures. The N 1s binding energy peak of N-doped TiO_2 heterojunctions were found to be highly depends on the calcination temperature. In the case of samples calcined at 700 °C, formation of N−Ti−N bonds were observed as a peak at 396 eV (which corresponds to an additional FT-IR peak at 415 cm^{-1}) (Figure 7 b).[38] This can be due to the formation of specific Ti−N bonds through an oxygen vacancy compensation mechanism at a higher temperature. Only one peak was observed at 400.1 eV in samples calcined at 600 °C (Figure 7 a), which is a value greater than the typical N 1s binding energy of 397.2 eV in TiN.[39] Since FT-IR and XRD results indicate lattice doping, this peak therefore can be attributed to the 1s electron binding energy of the N atom in the environment of O−Ti−N in lattice N-doped titania. The binding energy shifting can be understood by the fact that the N 1s electron binding energy is higher when the formal charge of N is more positive (e.g., 408 eV in $NaNO_3$), compared to zero or a negative formal charge (398.8 eV in NH_3).[39,40] When a nitrogen substitutes for the oxygen in the initial O−Ti−O structure, the electron density around N is reduced compared to that in a TiN crystal (because of the O atom on the Ti atom). Thus the N 1s binding energy in an O−Ti−N environment (400.1 eV) is higher than that in an N−Ti−N environment (396 eV) where the N atom replaces the O atom. These observations are consistent with the earlier XPS characterization results associated with the oxidation of TiN surfaces by Saha and Tomkins.[39]

As reported by Saha and Tomkins, pure titania sample has a typical Ti 2p binding energy of 459.4 eV.[39] A decrease of 0.35 and 0.96 eV in Ti 2p binding energy was observed for N-doped heterojunctions obtained at 600 and 700 °C, respectively, in comparison to the standard sample (Figure 8). A decrease of Ti 2p binding energy is a direct measure of the lowering of the valence state level of Ti^{4+} to Ti^{3+} and Ti^{2+} level as a result of the lattice substitution of nitrogen for oxygen.[35,41] Lattice incorporation of nitrogen creates Ti−N bonds by the partial replacement of O^{2-} with N^-. This results in an electron density decrease and partial reduction of Ti^{4+} to Ti^{3+} and Ti^{2+}, which reflects as a decrease in Ti 2p binding

---

(37) Jackson, A. W.; Shebanova, O.; Hector, A. L.; McMillan, P. F. *J. Solid State Chem.* **2006**, *179*, 1383–1393.

(38) Irie, H.; Watanabe, Y.; Hashimoto, K. *J. Phys. Chem. B* **2003**, *107*, 5483.

(39) Saha, N. C.; Tomkins, H. C. *J. Appl. Phys.* **1992**, *72*, 3072.

(40) Chen, X.; Burda, C. *J. Phys. Chem. B* **2004**, *108*, 15446–15449.

(41) Hashimoto, S.; Murata, A.; Sakurada, T.; Tanaka, A. *J. Surf. Anal.* **2002**, *9*, 459.

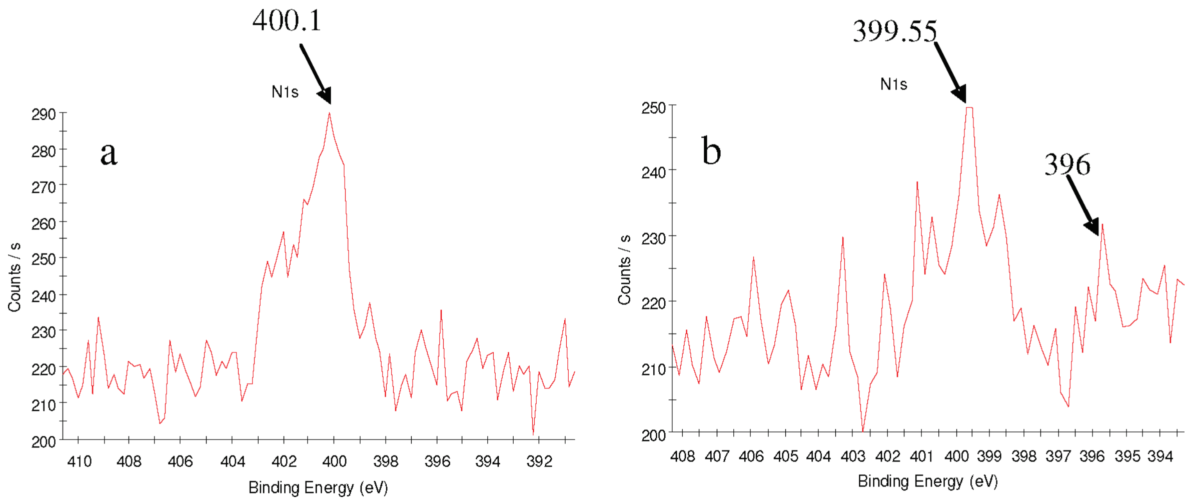

Figure 7. N 1s peaks in the XPS plot of calcined titania. (a) 0.5 ED-TiO_2 600, (b) 0.5 ED-TiO_2 700.

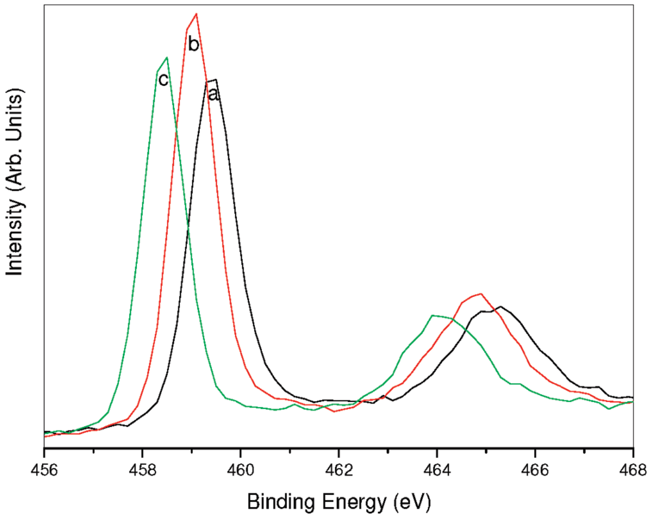

Figure 8. Ti 2p peaks in the XPS plot of calcined titania. (a) Control TiO_2 600, (b) 0.5 ED-TiO_2 600, (c) 0.5 ED-TiO_2 700.

Table 1. Band Gap Values of Heterojunctions Calcined at Different Temperatures

composition	band gap (eV) 400 °C	band gap (eV) 600 °C	band gap (eV) 700 °C
control TiO_2	3.11	3.16	3.15
0.5 ED-TiO_2	3.03	3.02	2.98
1.0 ED-TiO_2	3.00	3.00	2.96
1.5 ED-TiO_2	2.98	2.98	2.95
2.0 ED-TiO_2	3.05	2.97	2.93

energy.[41] An additional O 1s peak appeared for N-doped heterojunctions at 532 eV (Supporting Information 10), which was first observed by Saha and Tomkins and most recently characterized by Gyorgy et al. in their depth profiling study on TiN surfaces. Gyorgy et al. assigned this feature to the formation of oxidized TiN, which leads to the Ti−O−N structure.[42] Our study suggests that the appearance of this peak is a consistent feature for the nitrogen substitution in TiO_2 and signifies the formation of O−Ti−N and N−Ti−N structures. Moreover, Rodriguez et al. measured the O 1s peak for -NO and -NO_2 at 533.5 eV,[43] compared to the 532 eV value in our study, which can exclude the novel properties related to surface adsorbed nitrogen species. The presence of adventitious elemental carbon was also identified in samples (peak at 285 eV), (Supporting Information 11) which is an unavoidable presence on all air-exposed materials.[44] It is therefore clear from the above observations that the lowering of Ti 2p binding energies and additional O 1s peak observed for N-doped heterojunctions together with FT-IR and XRD results well explained successful lattice incorporation of nitrogen through the formation of O−Ti−N and N−Ti−N bonds.

3.2.5. UV/vis Spectroscopic Studies. Band gap values calculated through diffuse reflectance measurements also support the variations of nitrogen and rutile concentrations in heterojunctions. All N-doped heterojunctions show narrowing of the band gap in comparison to the control sample (Table 1). The narrowing effect was comparatively high for the composition 0.5 ED-TiO_2, which contain the highest amounts of nitrogen at each calcination temperature (Figure 9). Band gap narrowing effect was very low for compositions containing higher amounts of EDTA. This can be due to decreased N-doping as a result of excessive crystallite growth on increasing EDTA concentration. It was previously reported that the nitrogen doping can lead to a mixing of N 2p orbitals with O 2p orbitals to form intermediate energy levels and shift the absorption edge toward visible light region.[14,45] Nitrogen doping also accelerate the formation of oxygen vacancies, which form additional energy levels below the conduction band. This promotes electronic excitation from the valence band to the additional energy level by absorbing visible light.[46] A lowering of band gap values through

---

(42) Gyorgy, E.; Pino, A. P. d.; Serra, P.; Morenza, J. L. *Surf. Coat. Technol.* **2003**, *173*, 265.

(43) Rodriguez, J. A.; Jirsak, T.; Dvorak, J.; Sambasivan, S.; Fischer., D. *J. Phys. Chem. B* **2000**, *104*, 319.

(44) Sakthivel, S.; Kisch, H. *Angew. Chem., Int. Ed.* **2003**, *42*, 4908–4911.

(45) Morikawa, T.; Asahi, R.; Ohwaki, T.; Aoki, K.; Taga, Y. *Jpn. J. Appl. Phys.* **2001**, *40*, L561.

(46) Yang, J.; Bai, H.; Tan, X.; Lian, J. *Appl. Surf. Sci.* **2006**, *253*, 1988–1994.

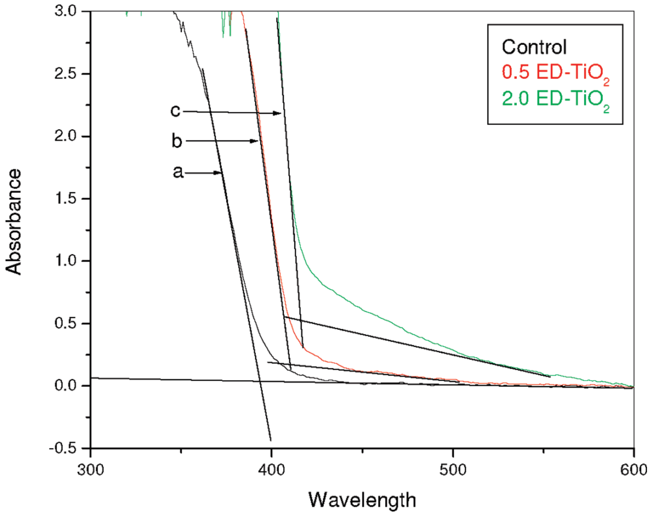

Figure 9. Diffuse reflectance spectra of (a) Control TiO_2 600, (b) 0.5 ED-TiO_2 600, and (c) 2.0 ED-TiO_2 600.

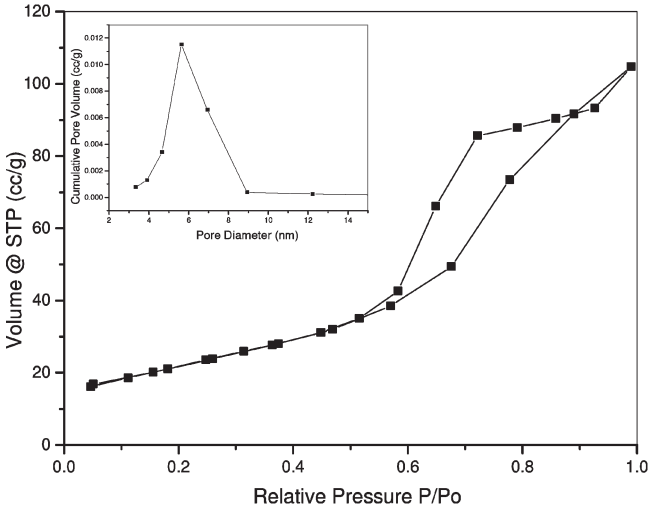

Figure 10. N_2 adsorption−desorption isotherm and the pore size distribution (inset) of 1.5 ED-TiO_2 400.

both of these mechanisms highly depends on the dopant concentration, which explains the band gap variations observed above.

The amount of rutile also plays a significant role to shift the absorption edge of heterojunctions toward the visible light region. Since it is evident from the XPS results that the amount of nitrogen decreases on increasing the EDTA content, a decrease in the band gap after the composition 0.5 ED-TiO_2 happens mainly because of rutilation. For this reason, all samples show a decrease in the band gap on increasing the calcination temperature. At 400 °C, band gap narrowing effect was low because of less rutilation at lower temperatures. The superior visible light absorbing capability of heterojunctions and their dependence on the amount of nitrogen and rutile were thus verified from diffuse reflectance results.

3.2.6. Surface Area Measurements. Isotherms of heterojunctions and the control sample show type IV characteristics with H1 type (cylindrical shape) of hysteresis (Figure 10).[47] The high steepness hysteresis loop ending at a relative pressure (P/P_0) of 0.6 is a measure of high order of mesoporosity in these samples.[48] Degussa P-25, the standard photocatalyst, has a type II isotherm with small hysteresis behavior (Figure 11). This fact demonstrates the presence of a large quantity of agglomerated particles formed through a diffusion process, which decreases the porosity. Among the different samples compared, the control sample has the highest surface area (134 m^2/g) and pore volume (0.209 cc/g) at 400 °C (Table 2). All heterojunction samples have lower surface area compared to the control sample at all calcination temperatures. For both heterojunctions and the control sample, a considerable decrease in surface area and pore volume was observed with an increase in calcination temperature.

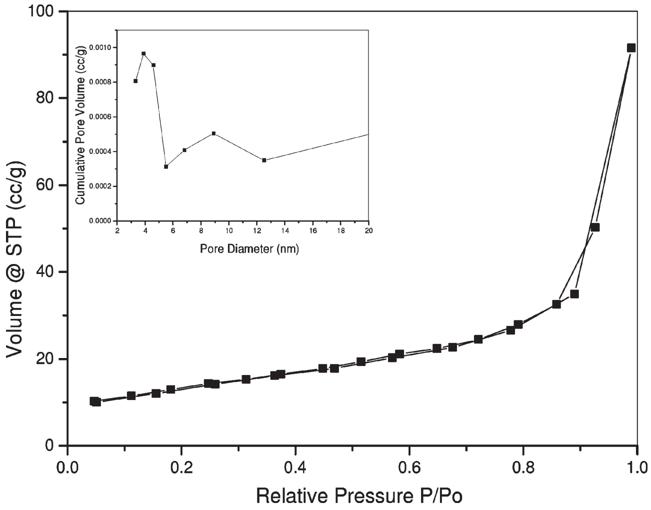

Figure 11. N_2 adsorption−desorption isotherm and the pore size distribution (inset) of Degussa P-25.

Table 2. Textural Properties of Heterojunctions Calcined at Different Temperatures

composition	surface area (m^2/g)	pore diameter (nm)	pore volume (cc/g)
control 400	134.2	4.65	0.209
control 600	40.06	8.16	0.104
1.5 ED-TiO_2 400	79.6	5.64	0.168
1.5 ED-TiO_2 600	21.28	8.01	0.052
Degussa P-25	46.7	3.89	0.129

An increase in pore diameter was also observed with an increase in calcination temperature, which confirms the presence of interstitial pores and its grain growth.[47] Among the samples calcined at 400 °C, the most active catalyst (1.5 ED-TiO_2) showed a larger pore diameter (5.6 nm) than the control sample (4.6 nm) because of the large grain size resulting from the thermally less stable titania precursor. The same composition has a smaller pore size at 600 °C compared to the control sample. This can be due to the densification of powder resulting from excessive grain growth. Even though the heterojunctions have poor

---

(47) Nasar, R. S.; Cerqueira, M.; Longo, E.; Varela, J. A. *Cerâmica* **2008**, *54*, 38–42.

(48) Kartini, I.; Meredith, P.; Costa, J. C. D. D.; Lu, G. Q. *J. Sol-Gel Sci. Technol.* **2004**, *31*, 185–189.

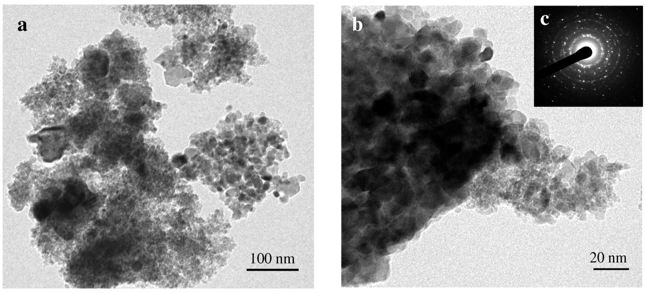

Figure 12. Transmission electron micrograph of 1.5 ED-TiO_2 400. (a) TEM, (b) HRTEM, and (c) SAED pattern.

textural properties in comparison to that of the control sample, properties of the most active heterojunction (1.5 ED-TiO_2 400) were superior to that of Degussa P-25. Better textural properties of the control sample arise because of the formation of thermally stable acetic acid-Ti^{4+} complex,[28] and lower textural properties of heterojunctions result from poor thermal stability of ionic intermediate formed by the reaction between Ti $^{4+}$ and EDTA.

3.2.7. Transmission Electron Microscopic Studies (*TEM*). The nanocrystalline structure and phase composition of the most active heterojunction (1.5 ED-TiO_2 400) had been investigated by combined high resolution transmission electron microscopy (HRTEM)-selected area electron diffraction (SAED) analysis as shown in Figure 12. The sample was found to be consisting of nanoparticles having two different sizes. The average particle size of about 90% of the particles was 10 ± 3 nm, and the remaining 10% were about 15 ± 3 nm in size. These results were consistent with the average crystallite size and anatase-rutile ratio obtained from the XRD analysis (90% 13 nm sized anatase and 10% 18 nm rutile). The 15 nm sized rutile nanoparticles were found to be distributed between anatase nanoparticles and thereby facilitate the formation of heterojunctions (Figure 12 a, b). The selected area electron diffraction (SAED) pattern contains a series of Debye−Scherrer rings that correspond to an anatase-rutile mixture (Figure 12 c). The *d*-spacing values 3.38, 2.23, 1.70, and 1.22 Å calculated from the pattern represent the anatase lattice planes with Miller indices (1 0 1), (0 0 4), (1 0 5), and (2 0 4), respectively.[49,50] The rutile lattice planes (1 1 0), (1 0 1), (1 1 1), and (2 2 0) were also identified from the corresponding *d*-spacing values of 2.90, 2.5, 2.1, and 1.59 Å.[49,50] The complex SAED ring pattern confirmed the presence of polycrystalline anatase and rutile nanoparticles oriented in a random manner.[50]

3.3. Photocatalytic Studies. *3.3.1. Visible Light Photocatalytic Degradation of MB over TiO_2 Heterojunctions.* All N-doped heterojunctions were more visible light active than the control sample or EDTA modified samples with a single phase toward the photocatalytic degradation of methylene blue. The most active heterojunction 1.5 ED-TiO_2 400 containing 90% of 13 nm anatase and 10% of 18 nm rutile shows over 9 times more visible light activity compared to Degussa P-25 (Figure 13 a, b). Rate constants obtained for the most active catalyst and Degussa P-25 were 0.038 and 0.004 min^{-1}, respectively (Figure 14). Significantly higher visible light activity of nitrogen doped anatase rutile heterojunctions can be explained on the basis of band gap narrowing and efficient charge separation at the anatase-rutile interface. Results obtained from XRD, FT-IR, XPS, and UV/vis spectroscopy confirmed the formation of N-doped anatase-rutile heterojunctions having low band gap values. Additional energy levels created as a result of efficient doping can utilize visible light for the generation of electron hole pairs. Asahi et al. explained the visible light sensitization of N-doped TiO_2 on the basis of Ti−N bonding. Irie et al. also prepared N-doped TiO_2 by a NH_3-treatment method.[38] They observed the N 1s peak at 396 and 400 eV in the XPS analysis and ascribed the 396 eV state to visible light sensitization. However, the results of Diwald et al. rather indicated a negative contribution of Ti−N bonding to photocatalytic activity.[51] So, the contribution of Ti−N bonding to the visible-light sensitization of TiO_2 has not been completely understood. In our experiments, all nitrogen doped anatase rutile mixtures at 700 °C with lower nitrogen content (containing N−Ti−N bonds) show better (except 1:0.5 ED-TiO_2) photocatalytic activity compared to samples at 600 °C (containing O−Ti−N bonds) (Supporting Information 12). This behavior can be correlated to the formation of higher amounts of photocatalytic enhancing Ti−N bonds at a higher temperature. The discrepancy observed in the case of 1:0.5 EDTA composition may be due to the presence of higher amounts of rutile at 700 °C.

In spite of its better textural properties, the control sample was found to have very low visible light activity compared to the most active sample, which has poor textural properties but high visible light activity. It is therefore evident from the photocatalytic studies that the textural properties of catalysts are not the only factor determining the reaction kinetics. It can be concluded that the composition of heterojunctions and band gap values contribute more toward the photocatalytic activity in comparison to the textural properties.

Crystallite sizes of anatase and rutile phases were smaller for the most active heterojunction (1.5 ED-TiO_2 400) than that in Degussa P-25 (Supporting Information 14). This facilitates the formation of more heterojunctions and thereby increases the activity. It is known that the conduction band edge of rutile is approximately 0.2 eV lower than that of anatase. On this basis, the model that the photo excited electrons (from the visible midgap level) are effectively transferred from the conduction band of anatase to that of rutile has been proposed (Figure 16). When a small amount of rutile phase coexists with anatase phase, the interface between anatase and

---

(49) Miao, L.; Jin, P.; Kaneko, K.; Terai, A.; Nabatova-Gabain, N.; Tanemura, S. *Appl. Surf. Sci.* **2003**, *212*, 255.

(50) Miao, L.; Tanemura, S.; Kondo, Y.; Iwata, M.; Toh, S.; Kaneko, K. *Appl. Surf. Sci.* **2004**, *238*, 125.

(51) Diwald, O.; Thompson, T. L.; Goralski, E. G.; Walck, S. D.; Yates, J. T. *J. Phys. Chem. B* **2004**, *108*, 52.

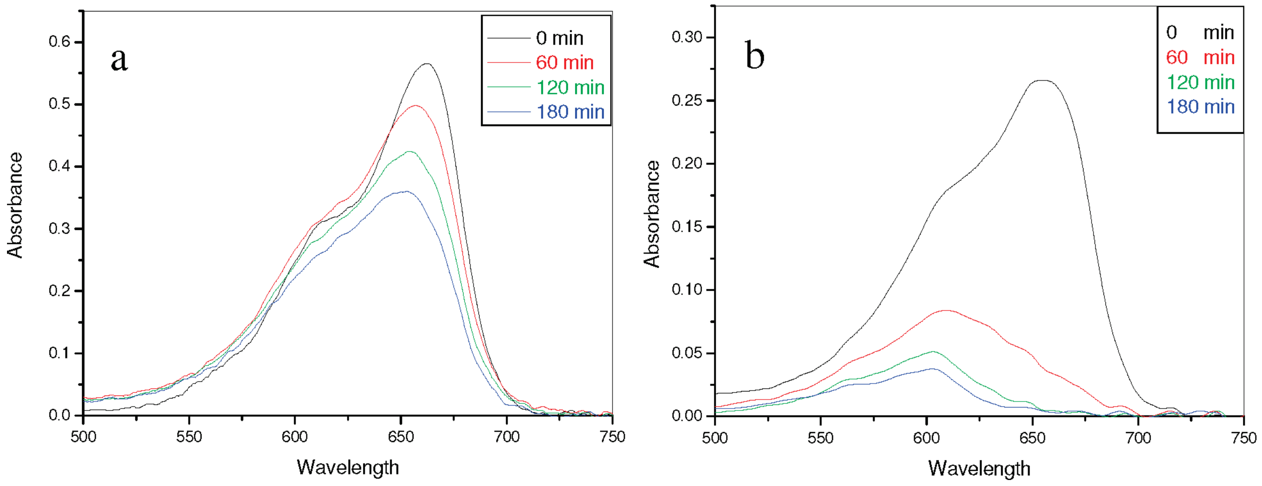

Figure 13. Absorption spectra of visible light induced methylene blue degradation using (a) Degussa P-25 and (b) 1.5 ED-TiO_2 400.

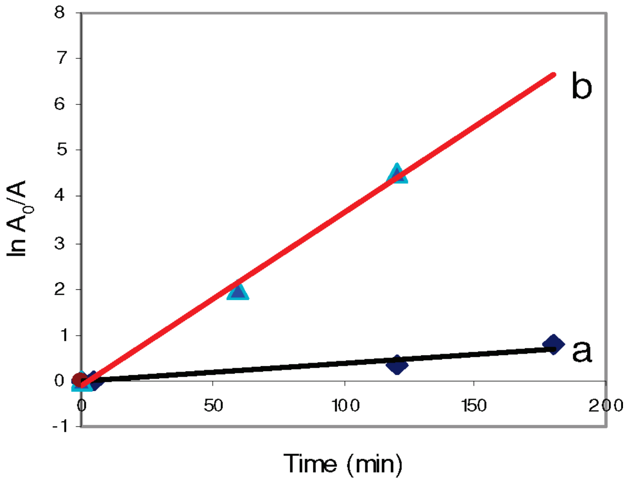

Figure 14. Kinetic study of (a) Degussa P-25 and (b) 1.5 ED-TiO_2 400.

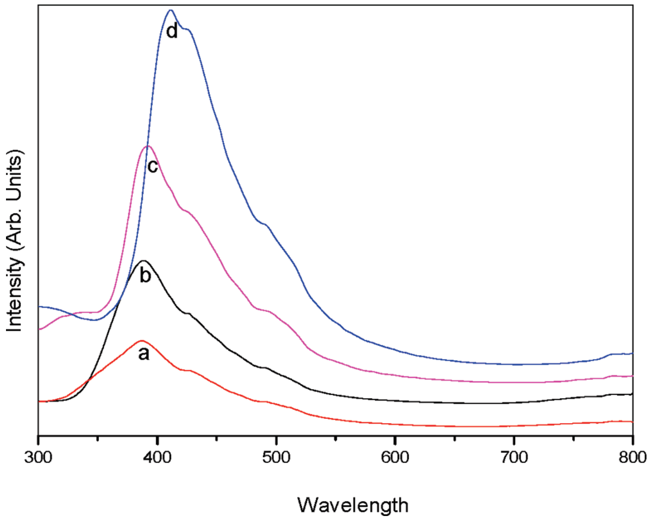

Figure 15. Photo luminescence spectra of samples (a) 1.5 ED-TiO_2 400, (b) Degussa P-25, (c) pure anatase, and (d) pure rutile.

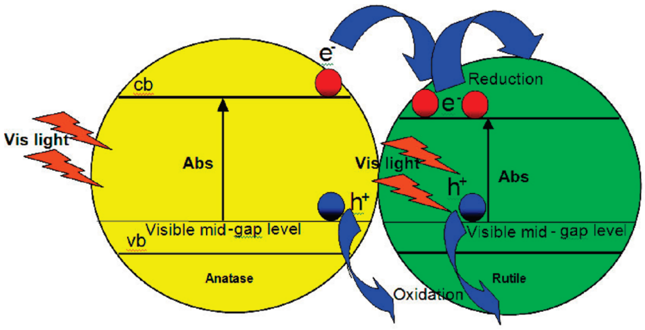

Figure 16. Electron transfer mechanism in N-doped anatase rutile heterojunction.

rutile promotes the electron transfer, and rutile works as a reaction site for photo reduction. Photo oxidation can take place either on anatase or on the rutile surface. The heterojunctions obtained at 700 °C containing more Ti—N bonds showed a higher photocatalytic activity in comparison to those obtained at 600 °C. The most active heterojunction was the one obtained at 400 °C, and its highest activity was found to be as a result of optimum anatase-rutile composition, nanocrystalline nature, and nitrogen doping. A decrease in photocatalytic activity was observed for heterojunctions synthesized at higher temperatures (Supporting Information 12). This can be due to the formation of a higher amount of rutile phase having higher electron hole recombination rate, and decreases in the amount of more photoactive anatase phase, nitrogen content, and surface area. Higher blue shift of methylene blue absorption peaks during the photocatalytic experiment of heterojunction samples indicates faster dye degradation through a N-demethylation mechanism.[52,53] The higher visible light photocatalytic activity observed for the heterojunctions can be therefore, correlated to the combined band gap narrowing effect of the nitrogen and electron hole separating effect of rutile.

3.3.2. Luminescence Studies. Information regarding the presence of surface states, formation of photo induced charge carriers, and their recombination kinetics can be drawn from the photoluminescence (PL) spectrum of a

---

(52) Zhang, Y.; Xu, H.; Xu, Y.; Zhang, H.; Wang, Y. *J. Photochem. Photobiol., A* **2005**, *170*, 279.
(53) Yu, J. R.; Hoi, W. C. *Environ. Sci. Technol.* **2008**, *42*, 294–300.

semiconductor material.[54] The phenomenon of photocatalysis involves a competitive formation of electron hole pairs and their recombination (radiative or nonradiative). Since defect concentration and life times of photoexcited species play an important role in photocatalysis, investigation of photocatalysts through PL spectroscopy is important to obtain critical reasons behind the enhanced photocatalytic activity. A strong correlation between PL intensity and photocatalytic activity was established by previous research.[54,55]

Among different samples, pure rutile has highest band−band PL intensity followed by pure anatase, Degussa P-25, and 1.5 ED-TiO_2 400 (Figure 15). Band-band PL intensities mainly depend on the extent of photoinduced charge carrier separation. The lower band gap and higher surface defects of rutile sample accelerate charge carrier recombination, which reflects as the most intense band−band PL peak.[56] Efficient electron hole separation resulting from a wider band gap and smaller crystallite size makes anatase less luminescent in comparison to rutile. The lower PL intensity of Degussa P-25 (which is a mixture of 70% anatase and 30% rutile) can be explained on the basis of better electron hole separation resulting from the electron transfer from the conduction band of anatase to that of rutile.[7] The slight red shift of the band−band transition observed for Degussa P-25 may be due to the presence of more rutile. Among the different N-doped heterojunctions, the lowest PL intensity was observed for sample 1.5 ED-TiO_2 400. The optimum phase composition (90% anatase +10% rutile) and nanocrystalline nature of components (which facilitates the formation of more heterojunctions) helps the effective transfer of photo excited electrons from anatase to rutile and slows down the recombination process. Also photoexcited electrons formed on rutile can be transferred to the defect states of anatase, promoting effective charge carrier separation. These processes are responsible for the lower PL intensity and very high photo activity of EDTA modified sample (1.5 ED-TiO_2 400). Excitonic intensities also follow the same order of band−band intensities because of the same reasons. No additional PL bands from nitrogen impurities were observed for heterojunctions, which eliminated the presence of surface adsorbed nitrogen impurities.

Lower band−band and excitonic PL intensities resulting from efficient charge separation were reported for TiO_2 and ZnO doped with Sn, W, Ag, and Au.[55,57−61] These semiconductors showing lower PL intensities were also reported to exhibit higher photocatalytic activity.[59,62] In short, any electron capturing agents can lower both the band−band and the excitonic PL intensities, which results in an increase in photocatalytic activity. Thus, the lowest PL intensity and the very high visible light activity of nitrogen doped anatase rutile heterojunctions can be explained on the basis of efficient charge separation at the anatase-rutile interface. It is known that the conduction band edge of rutile is approximately 0.2 eV lower than that of anatase.[7,18] On this basis, the model that the photoexcited electrons (from the visible midgap level) are effectively transferred from the conduction band of anatase to that of rutile has been proposed.

4. Conclusions

Nitrogen doped anatase-rutile heterojunctions having high visible light photocatalytic activity were developed through an ionic intermediate [Ti (H_2O) (edta)]. Low temperature crystallizations of heterojunctions were characterized using DSC, TGA, XRD, HRTEM, and Raman techniques. The nature of dopants was investigated using FT-IR spectroscopy, XRD, and XPS techniques. Conclusive evidence for the formations of both O−Ti−N and N−Ti−N bonds were observed from FT-IR and XPS studies, and substitutional nitrogen doping was found to have an enhancing effect on the photocatalytic activities of heterojunctions. The most active N-doped heterojunction obtained at 400 °C showed a 9-fold enhancement for the visible light decomposition of methylene blue in comparison to the commercial catalyst Degussa P-25. The heterojunction has lower luminescence intensity as a result of better electron hole separation, and better textural properties in comparison to Degussa P-25. The highest photocatalytic activity of the optimum sample (1.5 ED-TiO_2 400) was due to the combined effect of better electron hole separation, a lower band gap resulting from effective nitrogen doping, and nanocrystalline nature compared to the standard photocatalyst.

Acknowledgment. The authors would like to thank Enterprise Ireland for funding (CFTD/06/IT/326) and Dr. John Colreavy (Director, Centre for Research in Engineering Surface Technology) and Dr. Niall Stobbie for reviewing the paper. The authors would like to dedicate this paper to Professor John M. Kelly, on the occasion of completing his 37 years of teaching and research (celebration of chemistry) at Trinity College Dublin, Ireland.

Supporting Information Available: Further details are given in the supporting tables 1−3 and figures 1−13. This material is available free of charge via the Internet at http://pubs.acs.org.

---

(54) Liqiang, J.; Yichun, Q.; Baiqi, W.; Shudan, L.; Baojiang, J.; Libin, Y.; Wei, F.; Honggang, F.; Jiazhong, S. *Sol. Energy Mater. Sol. Cells* **2006**, *90*, 1773–1787.

(55) Georgekutty, R.; Seery, M. K.; Pillai, S. C. *J. Phys. Chem. C* **2008**, *112*, 13563–13570.

(56) Gandhe, A. R.; Fernandes, J. B. *J. Solid State Chem.* **2005**, *178*, 2953–2957.

(57) Shang, J.; Yao, W. Q.; Zhu, Y. F.; Wu, N. *Appl. Catal., A* **2004**, *25*, 257.

(58) Jing, L. Q.; Fu, H. G.; Wang, D. J.; Wei, X.; Sun, J. Z. *Acta Phys. Chim. Sin.* **2005**, *21*, 38.

(59) Li, X. Z.; Li, F. B.; Yang, C. L.; Ge, W. K. *J. Photochem. Photobiol., A* **2001**, *141*, 209.

(60) Xin, B. F.; Jing, L. Q.; Ren, Z. Y.; Wang, B. Q.; Fu, H. G. *J. Phys. Chem. B* **2005**, *109*, 2805.

(61) Li, F. B.; Li, X. Z. *Appl. Catal., A* **2002**, *228*, 15.

(62) Yu, J. G.; Yu, H. G.; Chen, B.; Zhao, X. J.; Yu, J. C.; Ho, W. K. *J. Phys. Chem. B* **2003**, *107*, 13871.